KSCE Journal of Civil Engineering (2019) 23(12):4992-5001

DOI 10.1007/s12205-019-0794-7

Geotechnical Engineering

pISSN 1226-7988, eISSN 1976-3808
www.springer.com/12205

Experimental Study on the Shear Behaviors of Polypropylene Fiber-Reinforced Sand

Gang Li*, Jinli Zhang, and Jia Liu*****

Received May 7, 2019/Revised June 26, 2019/Accepted September 2, 2019/Published Online November 5, 2019

Abstract

With excellent water permeability and high shear strength *S*, fiber-reinforced sand (FRS) is an ideal material for subgrades and has promising application prospects. In this study, the FRS were formed by adding the randomly distributed fibers to the sand specimens. Based on the triaxial consolidated drained tests, the effects of factors such as fiber content ζ, fiber length l_f, relative density D_r and confining pressure σ_3 on the *S* of FRS were systematically investigated. The test results showed that the *S* of the FRS increased as ζ, l_f, D_r and σ_3 increased. Under axial loads, the stress-strain curve of the FRS exhibited a hardening trend. Under specific D_r and σ_3, the *S* increment of the FRS had a strong linear relationship with ζ and l_f. The Mohr's stress circle results showed that the FRS possessed not only frictional strength but also high cohesive strength. Based on the triaxial consolidated drained test results, the *S* of the FRS was calculated using the Zornberg model and Michalowski model. The calculation results showed that the *S* predicated by the Zornberg model differed significantly from the measured values. However, the *S* predicted by the Michalowski model were in good agreement with the measured values.

Keywords: *fiber-reinforced sand, fiber length, fiber content, relative density, zornberg model, michalowski model*

1. Introduction

Weak subgrades are often encountered in transportation construction projects and, if left unreinforced, are prone to developing grave defects and, in severe cases, may affect the normal operation of roadways or railways. As reinforcing materials, geosynthetics (e.g., geogrids, geotextiles, geomembranes, geocells) have been extensively used and have achieved excellent results in foundation reinforcement and treatment. However, these geosynthetics share a common characteristic: when they are laid in layers in the soil, only the soil in contact with these reinforcing materials is reinforced, whereas the soil between the layers is left unreinforced and becomes a potential weak plane under a high load, resulting a major defect that must be addressed in engineering practice (Ding and Bao, 1999). Fiber-reinforced sand (FRS) is a type of composite material formed by adding a certain amount of fibers into the sand, where the fibers are randomly and evenly distributed and effectively contact the sand particles. The deformation of the soil in every direction is confined, and the development of a fracture plane is prevented by the inherent tensile strength of the fibers as well as the friction and interlocking between the fibers and the sand particles, thus increasing the shear strength *S* of the sand (Maher and Gary, 1990).

Research on the mechanical properties of FRS was carried out relatively early. In 1979, the French Central Laboratory of Roads and Bridges (Laboratoire Central des Ponts et Chaussées) began investigating the performance of geosynthetics in reinforcing sand particles and successfully applied the results in engineering practice, garnering the widespread attention of the geotechnical community. Later, extensive experiments were performed to study FRS. Shewbridge and Sitar (1989; 1990; 1996) carried out a detailed study on the development and deformation characteristics of shear bands in FRS in the condition of fiber were not randomly distributed in the sand by direct shear tests. They found that the shear band in FRS was wider than that in normal sand and grew larger as the FRS stiffness increased, and the increase in the strength of the FRS was not linearly related to the fiber content ζ. Yetimoglu and Salbas (2003) also examined the strength of FRS through direct shear tests and found that the peak shear strength and initial stiffness of the sand were not affected significantly by the fiber reinforcement. However, fiber could reduce its fracture toughness and maintain a high residual strength of the sand. Gray and Ohashi (1983) studied the mechanics behaviors of dry sand reinforced with different fibers by direct

*Associate Professor, Shaanxi Key Laboratory of Safety and Durability of Concrete Structures, Xijing University, Xi'an 710123, China (Email: T_bag945@126.com)

**Associate Professor, State Key Laboratory of Coastal and Offshore Engineering, Dalian University of Technology, Dalian 116024, China (Corresponding Author, Email: jlzhang@dlut.edu.cn)

***Ph.D. Candidate, School of Geological Engineering and Geomatics, Chang'an University, Xi'an 710054, China (Email: 15929935077@163.com)

shear test. Based on the experimental results, a force equilibrium model was used to predict the test. The results showed that fiber reinforcement increased the peak shear strength and limited post peak reductions, and the model could correctly predict the influence of parameters on the shear strength. Ahmad *et al*. (2010) studied the effects of various factors on the S of FRS through triaxial compression tests. They found that fiber content ζ, fiber length l_f significantly affected the S of the FRS. Li and Zornberg (2013) modified the Zornberg discrete model based on the experiment. They analyzed the peak and residual strengths of sand specimens and determined the coefficient of interaction using fiber pull-out tests. Sadek *et al*. (2010) compared the Zornberg discrete model and the Michalowski and Cermak energy dissipation model using direct shear tests and found that the Michalowski and Cermak model is effective in predicting the shear strength of FRS. Noorzad and Amini (2014) studied the effects of various parameters (ζ, l_f, D_r and σ_3) on the liquefaction resistance and shear modulus of FRS through 30 cyclic triaxial tests. They found that the FRS had significantly higher liquefaction resistance than normal sand, that the number of loading cycles needed to liquefy the FRS increased as ζ and l_f increased, and that the shear modulus of the FRS increased as ζ increased. Sadeghi and Beigi (2014) examined a linear elastic model for fiber-reinforced clayey sand (FRCS) through a series of dynamic triaxial tests. They found that the shear modulus decreased with increasing deviator stress ratio at high confining pressure, and the loss rate of shear modulus was much lower for FRCS. Furthermore, Consoli *et al*. (2003; 2005; 2009) carried out the plate load test, laboratory triaxial compression test and high-pressure isotropic compression test on fiber-reinforced soil to explore the mechanical behavior of the sand with randomly distributed polypropylene fibers. Ranjan *et al*. (1996) studied the fiber behaviors, soil behaviors and confining stress on the shear strength of reinforced soil with randomly distributed fibers by the triaxial compression test. Based on the test results, a mathematical model was established to take into account the influence of above factors on the shear strength. Claria and Vettorelo (2016) examined the shear strength and deformation behavior of loose sand reinforced with randomly oriented polypropylene by drained triaxial, direct shear and shear wave velocity tests. Tang *et al*. (2016) carried out the direct tensile test and desiccation test to explore the tensile strength of reinforced soil with randomly distributed polypropylene fibers. Shukla (2017) summarized a complete description of fibers effects on a soil or other similar materials, and their field applications. Wang *et al*. (2017) investigated the strength behaviors of expensive soil reinforced with jute fiber by direct shear test and triaxial compression tests, and found that the jute fibers could enhancing shear strength and deviator stress-strain behavior, and reducing the postpeak strength loss of expansive soil.

According to the above analysis, it can be concluded that most previous investigations have focused on the mechanical properties, deformation characteristics and reinforcing mechanism of fiber-reinforced sand. However, sand distribution exhibits typical regional characteristics, it is cost-effective and environmentally friendly to adopt local materials for engineering implication. In order to promote the implication of FRS, it is important to research on the mechanical properties of FRS with local sand. To date, relatively few studies have been conducted to examine the strength behavior of Dalian local sand with fiber-reinforced. In this study, through extensive laboratory triaxial consolidated drained tests, the effects of ζ, l_f, D_r and σ_3 on the S of FRS were analyzed. Based on triaxial test results, the S of FRS was predicted using the Zornberg model and Michalowski model.

2. Materials and Methods

2.1 Test Materials

Local river sand from Dalian was used in the tests. The sand was sieved through a 1-mm mesh sieve. The sieved sand was collected and washed with water and subsequently sieved through a 0.075-mm mesh sieve to remove the silty clay particles. After drying, the sand was subjected to a size distribution test, the results as shown in Fig. 1. The sand had a specific gravity G_s of 2.66, a maximum dry unit weight of 16.9 kN/m^3, a minimum dry unit weight of 13.0 kN/m^3, a coefficient of uniformity C_u of 3.36, a coefficient of curvature C_c of 0.89 and a median particle size D_{50} of 0.31 mm, thus characterized as poorly graded medium sand. HG-OX2 mortar polypropylene (PP) fibers manufactured by Jiangsu Yancheng Henggu Fiber Co., Ltd. were used in the tests. The fibers were well-dispersed beam-like monofilaments with a circular cross-section. Due to the FRS with fiber content

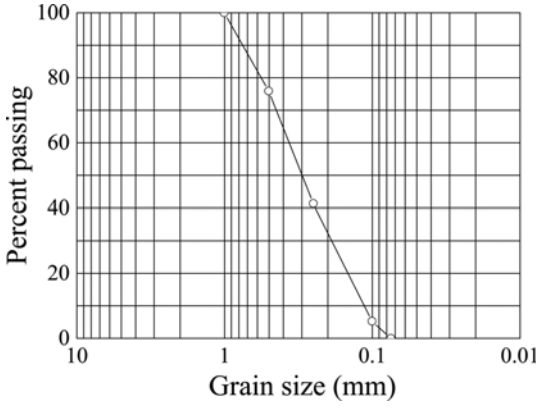

Fig. 1. Gradation Curve for Sand

Table 1. Physico-Mechanical Properties of Polypropylene

Parameters	Values
Linear density (dtex)	5.6
Diameter (mm)	0.025
Specific gravity	0.91
Tensile strength (MPa)	640
Tensile strain (%)	26.4
Elasticity modulus (MPa)	5870
Fusion point (°C)	>160
Ignition point (°C)	>580

of approximately 0.2 – 0.6%, which have a low engineering cost but marked economic benefits. Therefore, the fiber content used in this study is 0.2%, 0.4% and 0.6%, respectively. The length of HG-OX2 fibers are 7 mm, 13 mm and 19 mm, so three fiber length were used to analyze the effect on the strength behaviors of FRS. The physical and mechanical properties of the fibers are summarized in Table 1.

2.2 Specimen Preparation

To ensure an even distribution of fibers in the sand specimens, the number of specimens for each condition was estimated in advance. The required specimens were prepared in advance in one batch to ensure uniformity. After repeated tests, it was discovered that when the water content of the sand specimen was in the range of 5 – 7%, the fibers were prone to dispersion during the mixing process and could not easily absorb water to form strips. The preparation process is detailed as follows:

1. A certain amount of sand that had been sieved through a 0.075-mm mesh sieve was sufficiently dried and then weighed. Afterwards, the sand was mixed with water, and the mixture was stirred to prepare a sand specimen with a water content of 7%.
2. Based on the preset ζ, a corresponding mass of fibers was weighed. A small amount of fibers was dispersed in the sand specimen. After sufficient stirring, the fibers were distributed evenly. ζ was calculated using the following equation:

$$\zeta = \frac{m_f}{m_s} \times 100\% \tag{1}$$

where ζ is the fiber content (%), m_f is the mass of the fibers (kg), and m_s is the mass of the dry sand (kg).

3. The prepared FRS specimen was sealed with a plastic film and placed in a sealed box to prevent water loss. Before each test, a certain amount of the FRS was weighed, dried, and subsequently analyzed to determine its water content. To compensate for the measured decrease in water content, a suitable amount of water was then added to ensure that the water content of the specimen was 7% at the beginning of the test.
4. The specimens were made by wet packing, and the FRS weight was calculated by the specimen density and the specimen size. The FRS were weighted and divided into 4 parts, each part of FRS was accurately weighted to 0.01 g. Each part of FRS was placed into steel split mold, the layers were compacted in a 20 mm thickness. In order to ensure the consistency of specimens, the surface of each layer was scratched. After compaction the last layer, the scattered FRS was collected and pressed lightly on the top of the split mold with steel ruler.

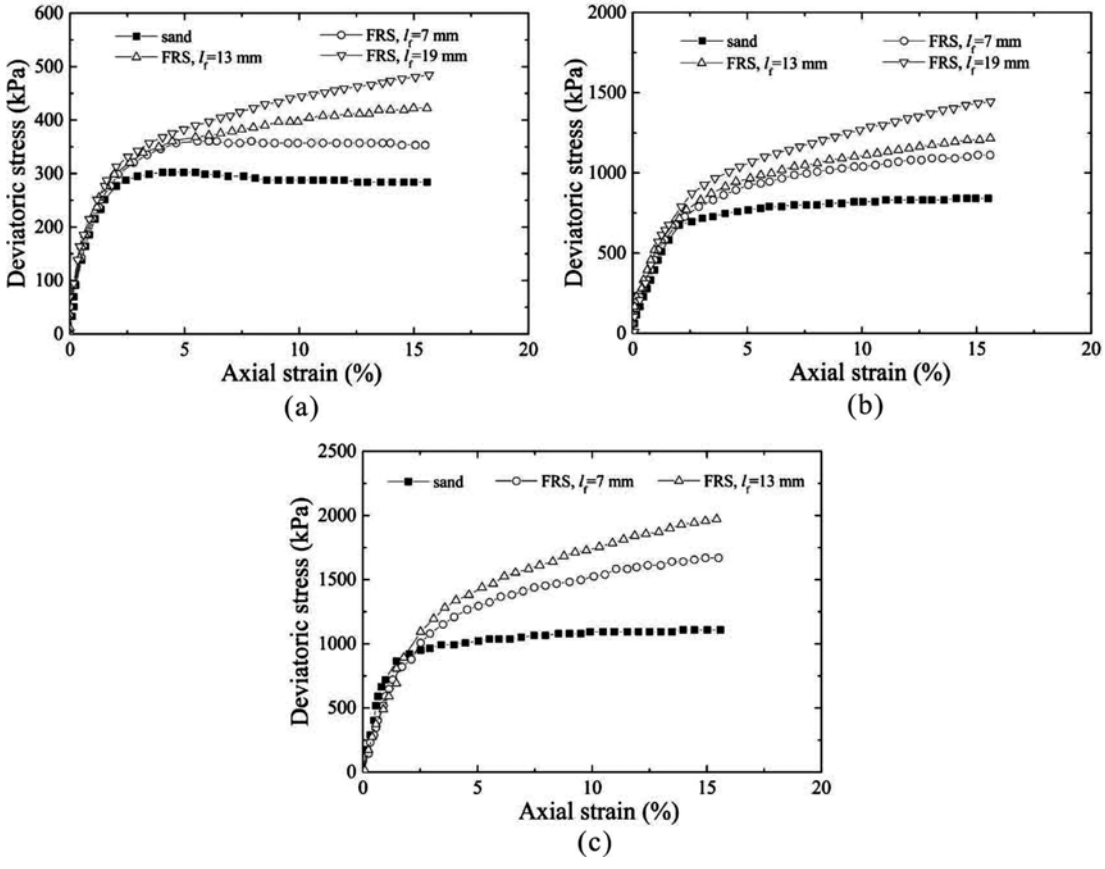

Fig. 2. Effects of Fiber Length on the Stress-Strain Curves: (a) D_r = 0.5, ζ = 0.2%, σ_3 = 100 kPa; (b) D_r = 0.6, ζ = 0.4%, σ_3 = 300 kPa, (c) D_r = 0.7, ζ = 0.6%, σ_3 = 400 kPa

2.3 Test Equipment and Methods

An SLB-1 type stress/strain-controlled triaxial shear permeameter (Nanjing Soil Instrument Factory Co., Ltd.) was used to perform triaxial consolidated drained tests on the FRS. Each FRS specimen had a diameter of 39.1 mm, a height of 80 mm, and was prepared using the wet tamping method. Each specimen was first saturated and then consolidated. The strain-controlled mode was used and the strain rate was set to 0.02 mm/min. The occurrence of the peak of deviatoric stress σ_d was used as the failure criterion. When there was no peak, an axial strain of 15% was used as the failure criterion.

3. Test Results and Analysis

3.1 Analysis of the Effects of l_f

At a fixed σ_3, D_r and ζ, the effects of l_f on the stress-strain curve of the FRS were analyzed by varying l_f. Due to a relatively large data volume, only three typical stress-strain curves are presented in Fig. 2. It is demonstrated that the stress-strain curve of the FRS exhibited a strain-hardening trend throughout the process, which conform to the other researchers' results (Li and Zornberg, 2013; Wang *et al*., 2017). It is suggested that under the axial load, the fibers underwent tensile deformation due to the lateral deformation of the specimen, and the tensile stress generated by the fibers confined the lateral deformation of the surrounding sand particles. As a result, a strain-hardening phenomenon was observed. Evidently, adding a certain amount of fibers significantly reinforced the sand. The main reason is that when the sand undergoes in the compacted state, the voids between sand particles reduce and the particles surface mainly contact together. When the fiber mixed with sand, the fiber strengthened the bond between the particle and effectively restrained deformation and displacement of the particles. Thereby, the shear strength of FRS remarkable increased.

3.2 Analysis of the Effects of ζ

The effects of ζ on the S of the FRS were comparatively analyzed by varying ζ while maintaining D_r, l_f and σ_3 at different values. As shown in Fig. 3, at fixed l_f, D_r and σ_3, the S of the FRS increased as ζ increased, which consistent with the other scholars' results (Li and Zornberg, 2013; Diambra *et al*., 2010; Ranjan *et al*., 1996; Wang *et al*., 2017; Wang *et al*., 2018). The stress-strain curves display a strain-hardening trend. The pattern of change in the stress-strain curve caused by changes in ζ is similar to that caused by changes in l_f. When ζ was low and l_f was short, the fiber presented the state of disjoint or partial intersection, and the fibers strengthened the cohesion between particles. Thereby, the shear strengths of FRS were improved by fiber tensile. When ζ was high, the fiber interface to form a network structure. The fibers mutually constrained when the

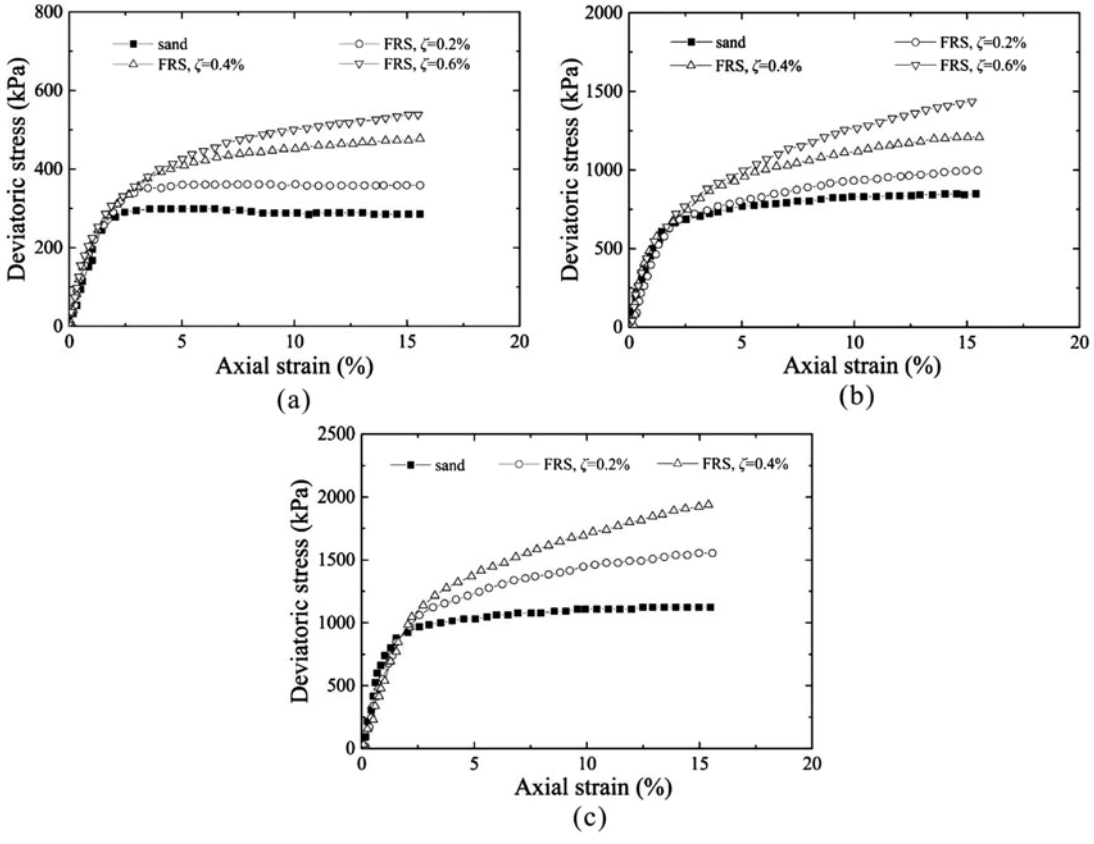

Fig. 3. Effects of Fiber Content on Stress-Strain Curves: (a) D_r = 0.5, l_f = 7 mm, σ_3 = 100 kPa; (b) D_r = 0.6, l_f = 13 mm, σ_3 = 300 kPa, (c) D_r = 0.7, l_f = 19 mm, σ_3 =4 00 kPa

displacement generated by external force, which resulted in the integrity improved. At a fixed l_f, the S of the FRS increased considerably as ζ increased from 0.2% to 0.4%. As ζ increased from 0.4% to 0.6%, the S of the FRS increased slightly at a large strain. Thus, to effectively increase the S of the FRS, selecting a suitable l_f and ζ is of paramount importance.

3.3 Analysis of the Effects of D_r

The strength of sand is related to its D_r. In engineering practice, FRS is required to have relatively high D_r when used as a subgrade. High D_r values (0.5, 0.6 and 0.7) were used to analyze the effects of the D_r of fibers. As shown in Fig. 4, when σ_3, ζ and l_f remained fixed, the S of the FRS increased as D_r increased, and that is consistent with the results of Michalowski and Cermak (2003). At various D_r values, in terms of initial tangent modulus, the stiffness of the sand decreased and its deformation increased after fibers were added. When the deformation of the sand exceeded its peak strain, the FRS still exhibited strain-hardening and did not soften, suggesting that fibers played their role only when the FRS underwent large deformation. Due to their high tensile strength (640 MPa), PP fibers undergo large deformation (26.4%) before tensile failure. Assuming that fibers are linear elastic materials, the tensile force generated by fibers increases in equal proportion to the increase in their deformation. Thus, when the FRS underwent large deformation, the tension resistance of the fibers was realized, thereby limiting the lateral deformation of the specimen. As a result, a continuous hardening phenomenon could be observed from the stress-strain curve.

3.4 Analysis of the Effects of σ_3

Figure 5 shows the σ_3-affected stress-strain curves of the FRS. The S of sand as a frictional material increased as σ_3 increased, which consistent with the results of Ahmad *et al*. (2010) and Michalowski and Cermak (2003). FRS is a type of composite material, and the role of the fibers in FRS can be realized only when they are stretched. In this study, considering that the FRS underwent not only axial deformation but also lateral deformation during the shear process, the fibers between the particles underwent the same deformation as the particles. When a specimen underwent lateral deformation, the fibers underwent tensile deformation. The resulting tensile stress limited the lateral deformation of the particles and thus improved the S. The higher the σ_3 value was, the higher the axial stress required for lateral deformation was, the greater the tensile deformation of the fibers was, the more significantly the fibers constrained the particles, and consequently, the higher the S of the FRS was.

3.5 Analysis of the S Parameters of the FRS

The strength of soil consists mainly of two parts, namely, cohesive strength c and frictional strength f ($f = \sigma \tan\varphi$). Generally, a

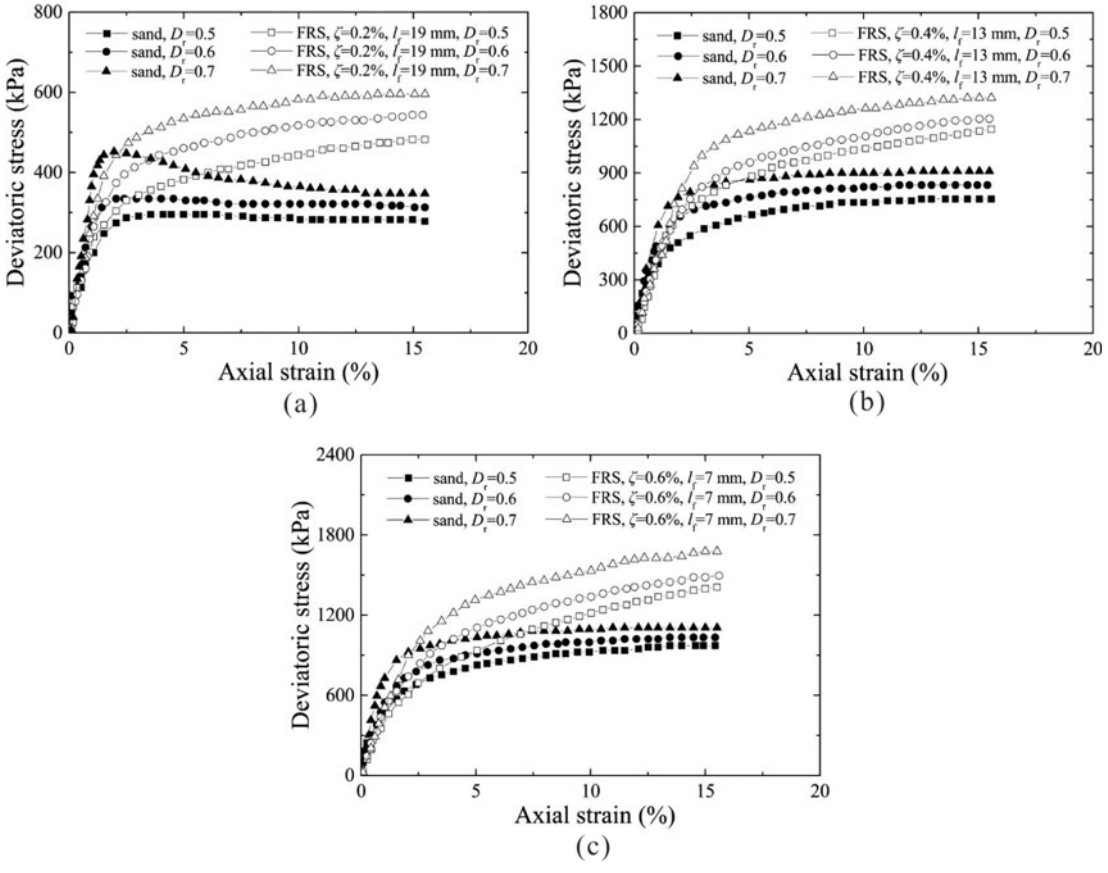

Fig. 4. Influences of Relative Density on the Stress-Strain Curves: (a) ζ = 0.2%, l_f = 19 mm, σ_3 = 100 kPa; (b) ζ = 0.4%, l_f = 13 mm, σ_3 = 300 kPa; (c) ζ = 0.6%, l_f = 7 mm, σ_3 = 400 kPa

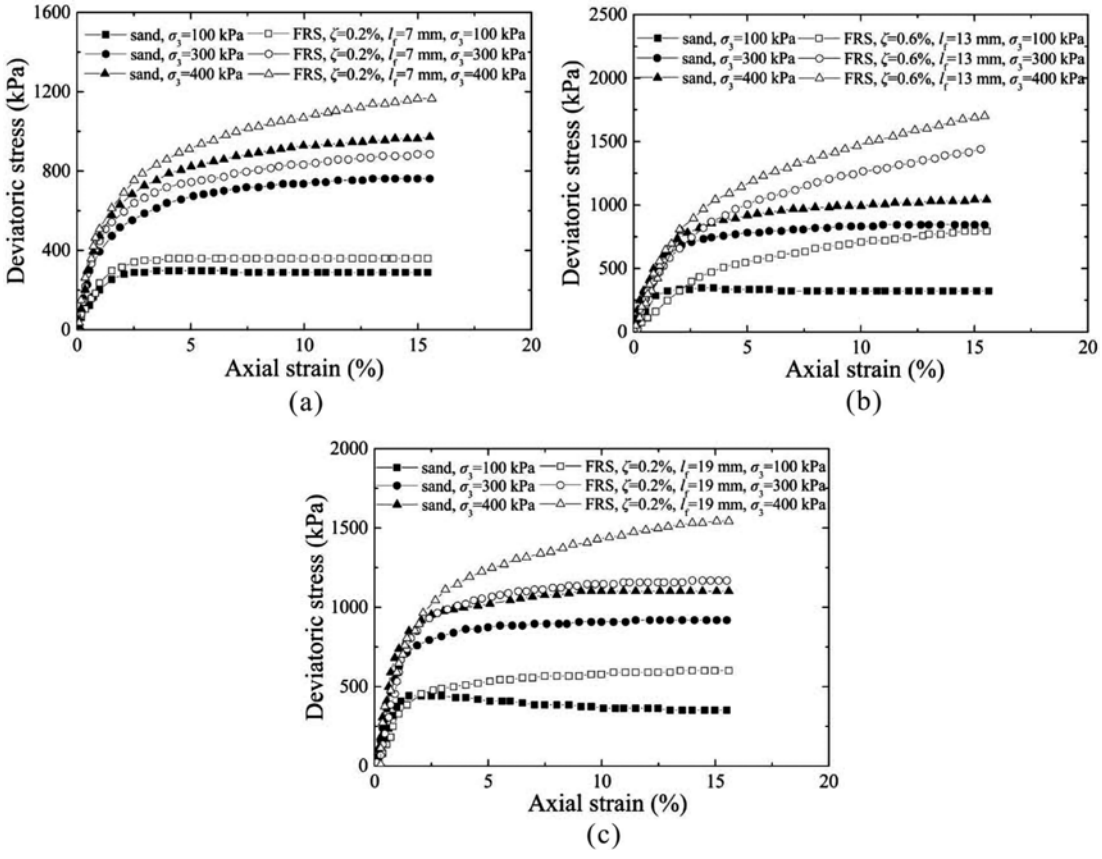

Fig. 5. Influence of Confining Pressure on the Stress-Strain Curves: (a) D_r = 0.5, ζ = 0.2%, l_f = 7 mm, (b) D_r = 0.6, ζ = 0.6%, l_f = 13 mm; (c) D_r = 0.7, ζ = 0.2%, l_f = 19 mm

Table 2. Shear Strength Parameters of Sand and Fiber-Reinforced Sands

Sand			FRS															
D_r	φ (°)	c (kPa)	ζ (%)	l_f (mm)	D_r	φ(°)	c (kPa)	ζ (%)	l_f (mm)	D_r	φ (°)	c (kPa)	ζ (%)	l_f (mm)	D_r	φ (°)	c (kPa)
0.5	33.4	0			0.5	34.4	25.6			0.5	35.2	45.9			0.5	36.2	62.1
0.6	34.6	1.4		7	0.6	35.2	31.2		7	0.6	36.4	58.9		7	0.6	37.3	64.0
0.7	36.4	7.3			0.7	36.7	33.8			0.7	37.2	69.5			0.7	38.8	80.8
					0.5	35.1	27.4			0.5	35.9	70.0			0.5	38.0	101.0
			0.2	13	0.6	36.0	37.4	0.4	13	0.6	36.6	79.4	0.6	13	0.6	39.1	107.8
					0.7	36.9	51.8			0.7	38.2	86.4			0.7	41.2	115.1
					0.5	36.1	50.0			0.5	37.5	91.8					
				19	0.6	36.9	66.0		19	0.6	38.9	100.0					
					0.7	37.8	69.0			0.7	40.3	102.7					

coarse-grained soil has no c and only f. FRS is a type of composite material, and in this study, its failure is assumed to follow the Mohr–Coulomb strength theory. Considering the effects of ζ, l_f and D_r, the triaxial test data were analyzed. Table 2 summarizes the S parameters for various conditions obtained by drawing a stress circle for the ultimate state. As demonstrated in Table 2, overall, after adding a certain amount of fibers, the angle of internal friction φ of the sand increased slightly, and its c became high, which conform to the results of Consoli *et al.* (2003). At a fixed ζ, the c provided by long fibers was greater than that provided by short fibers, and long fibers also led to a significant increase in φ. This is because the fibers were embedded between and closely interlocked with the sand particles during the shear process, limiting the relative dislocation of the sand particles; additionally, as the elastic reinforcement, the fibers provided tensile resistance, thereby increasing the c of the sand. The reinforcing mechanism of FRS can be summarized as bending mechanism and interweaving mechanism. Bending mechanism means that the distribution of fiber was composed of countless bending and turning points, and there were almost no straight segments. When the FRS subjected to external force and the fiber was pulled, the pressure and friction of the fiber on the sand

particles will be generated, thus strengthening the sand. Mixed mechanism means that fibers with disordered distribution exist countless interlacing point, if the fiber at the corner had the tendency of displacement, it will meet other fiber to stop the displacement, which forming a space stress area. Therefore, the reinforcing effect not only from the friction resistance between fiber and sand, but also from the spatial constraint effect of fiber network (Zhang *et al*., 2005).

4. Examination of Strength Models for FRSs

4.1 Zornberg Model

Zornberg (2002) assumed that fibers used to reinforce sand are evenly distributed in the sand and primarily reinforce the sand through their friction with the sand particles at the interface. The S_{eq} of FRS can be decomposed into two parts, namely, the tensile stress t of the fibers and the S of the sand, which can be represented by:

$$S_{eq} = S + t \tag{2}$$

where S_{eq} is the equivalent shear strength of the FRS, S is the shear strength of the sand, and t is the tensile stress of the fibers. There are two modes of failure for the fibers, namely, pull-out and rupture.

1. When the fibers undergo pull-out failure, calculations are performed using the following equations:

$$t_p = \alpha\chi\eta\left(c_{i,c}c + c_{i,\varphi}\sigma_{n,ave}\tan\varphi\right) \tag{3}$$

$$c_{i,c} = a/c \tag{4}$$

$$c_{i,\varphi} = \tan\delta/\tan\varphi \tag{5}$$

where $c_{i,c}$ and $c_{i,\varphi}$ are coefficients of interaction between the fibers and sand, representing cohesive and frictional actions, respectively; a and φ are the cohesion and angle of internal friction between the fibers and sand, respectively; χ and η are the volume and length/diameter ratio of the fibers, respectively; and α is the distribution direction coefficient of the fibers ($\alpha = 1$ for randomly evenly distributed fibers).

2. When the fibers undergo rupture failure, calculations are performed using the following equations:

$$t_t = \alpha\chi\sigma_{f,ult} \tag{6}$$

where $\sigma_{f,ult}$ is the tensile strength of the fibers. $\sigma_{n,ave} = (\sigma_1 + 2\sigma_3)/3$ is the average normal stress.

When the fibers undergo pull-out failure, the S_{eq} of the FRS can be represented by:

$$S_{eq,p} = c_{eq,p} + \tan\varphi_{eq,p}\sigma_{n,ave} \tag{7}$$

$$c_{eq,p} = \left(1 + \alpha\eta\chi c_{i,c}\right)c \tag{8}$$

$$\tan\varphi_{eq,p} = \left(1 + \alpha\eta\chi c_{i,\varphi}\right)\tan\varphi \tag{9}$$

Sand generally has no c. Thus, Eq. (7) can be rewritten to:

$$S_{eq,p} = \tan\varphi_{eq,p}\sigma_{n,ave} = \left(1 + \alpha\eta\chi c_{i,\varphi}\right)\tan\varphi\sigma_{n,ave} \tag{10}$$

$$\varphi_{eq,p} = \arctan\left[\left(1 + \alpha\eta\chi c_{i,\varphi}\right)\tan\varphi\right] \tag{11}$$

As demonstrated in Eq. (11), the S_{eq} of the FRS does not contain c but only f. φ_{eq} is the equivalent φ.

When the fibers undergo rupture failure, the S_{eq} of the FRS can be represented by:

$$S_{eq,t} = c_{eq,t} + \tan\varphi_{eq,t}\sigma_{n,ave} \tag{12}$$

$$c_{eq,t} = c + \alpha\chi\sigma_{f,ult} \tag{13}$$

$$\tan\varphi_{eq,t} = \tan\varphi \tag{14}$$

Similarly, $c = 0$. Thus, Eq. (12) can be rewritten as:

$$S_{eq,t} = \alpha\chi\sigma_{f,ult} + \tan\varphi\sigma_{n,ave} \tag{15}$$

4.2 Michalowski Model

Michalowski and Cermak (2003) assumed that FRS is a homogeneous, isotropic material and, based on energy dissipation, established an FRS strength model for the ultimate state. It is assumed that the energy dissipation rate of FRS is equal to the power exerted by the macroscopic stress, which can be represented by:

$$\bar{\sigma}_{ij}\bar{\dot{\varepsilon}}_{ij} = \frac{1}{V}\int D(\dot{\varepsilon}_{ij})dV \tag{16}$$

where V is the volume of the FRS and $\bar{\dot{\varepsilon}}_{ij}$ is the average strain rate.

When $\eta < \frac{1}{2}\frac{\sigma_0}{\sigma_n\tan\varphi_w}$ (where σ_0 is the tensile strength of the fibers; σ_n is the normal surface stress of the fibers; φ_w is the angle of internal friction of the FRS), it is considered that the fibers undergo sliding failure; otherwise, it is considered that the fibers undergo rupture failure.

1. When the fibers undergo pull-out failure, their failure criterion is as follows:

$$R = p\left(\sin\varphi + \frac{1}{3}N\rho\eta\tan\varphi_w\right) \tag{17}$$

$$N = \frac{1}{\pi}\cos\varphi + \left(\frac{1}{2} + \frac{\varphi}{\pi}\right)\sin\varphi \tag{18}$$

$$R = \sqrt{\frac{\left(\sigma_x - \sigma_y\right)^2}{4} + \tau_{xy}^2} \tag{19}$$

$$p = \frac{\sigma_1 + \sigma_3}{2} \tag{20}$$

φ_{eq} can be represented by:

$$\varphi_{eq} = 2\arctan\sqrt{\frac{1 + \sin\varphi + \frac{1}{3}N\rho\eta\tan\varphi_w}{1 - \sin\varphi - \frac{1}{3}N\rho\eta\tan\varphi_w}} - \frac{\pi}{2} \tag{21}$$

2. When the fibers undergo rupture failure, their failure criterion is as follows:

$$\frac{R}{\rho\sigma_0}=\frac{p}{\rho\sigma_0}+\frac{1}{3}N\left(1-\frac{1}{4\eta\rho}\frac{\cot\varphi_w}{\frac{p}{\rho\sigma_0}}\right) \tag{22}$$

where ρ and η are the volume content and length/diameter ratio of the fibers, respectively, and φ is the angle of internal friction of the sand.

Considering that fibers have relatively high tensile strength (the fibers used in the tests of this study had a tensile strength of 640 MPa), they did not undergo tensile failure under the loads selected in this study. Thus, pull-out was the mode of failure for the fibers in the abovementioned two models.

4.3 Comparison between the Test Results and Calculation Results

The parameters in the Zornberg model were mainly determined using the method recommended by Li and Zornberg (2013). Considering the level of evenness in distribution of fibers and the efficiency at which fibers play their role, the value of α ranges from 0.6 to 0.7. An α of 0.6 was used in the calculation. Based on the fiber pull-out test results, the coefficient of friction $c_{i,\varphi}$ between the fibers and sand was set to 0.30. The mass content of fibers used in the tests was set to 0.2%, 0.4% and 0.6%, respectively,

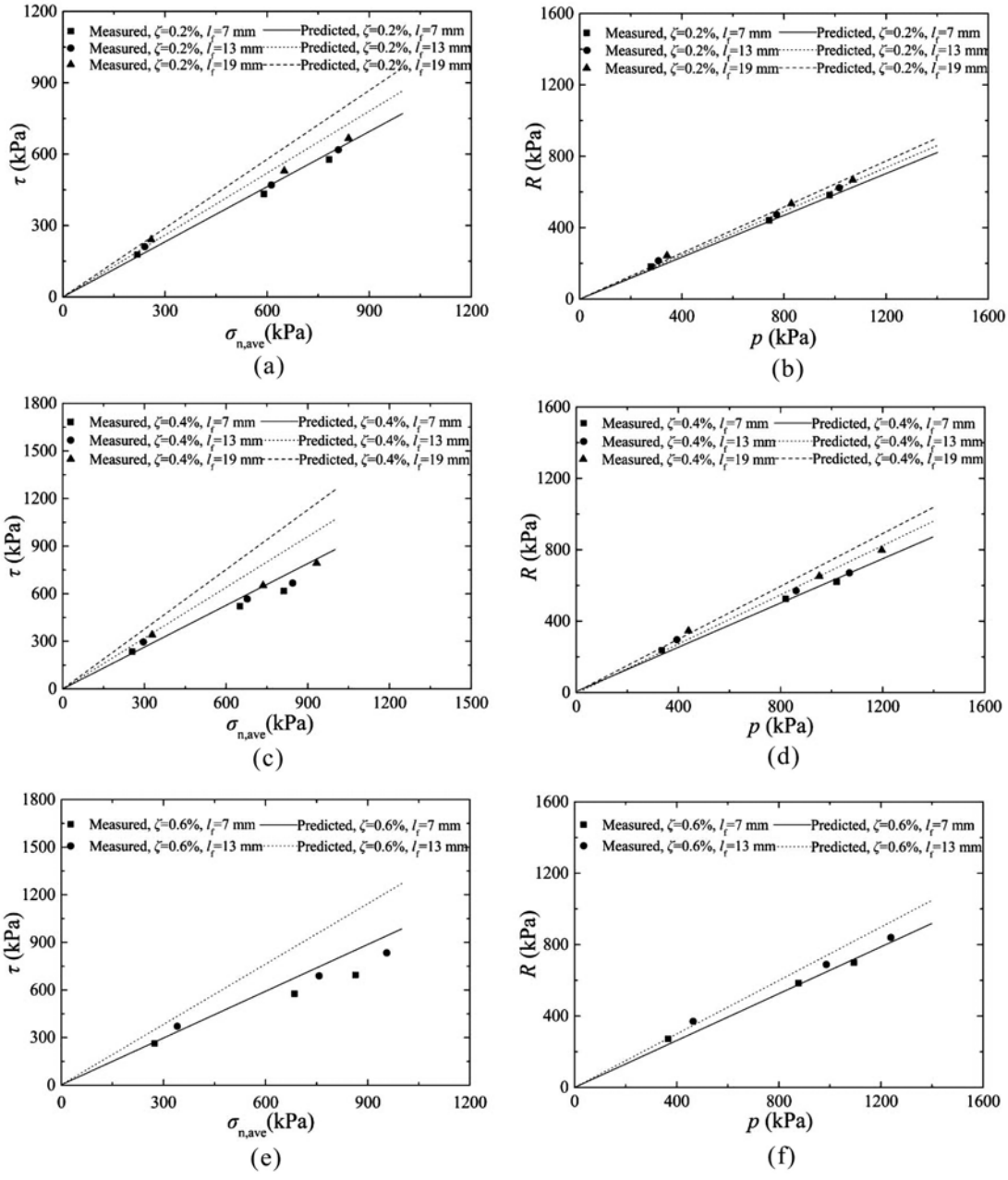

Fig. 6 Comparison of Strength Theory Model and Test Results (D_r = 0.5): (a) Zornberg Model (ζ = 0.2%), (b) Michalowski Model (ζ = 0.2%), (c) Zornberg Model (ζ = 0.4%), (d) Michalowski Model (ζ = 0.4%), (e) Zornberg Model (ζ = 0.6%), (f) Michalowski Model (ζ = 0.6%)

which was converted, based on the specimen volume, to a volume content of 0.332%, 0.664% and 0.996%, respectively. The η corresponding to a fiber diameter of 7, 13 and 19 mm was 280, 520 and 760, respectively. The parameter φ_w in the Michalowski model was indirectly calculated based on the equation of $\tan\varphi_w = c_{i,\varphi} \times \tan\varphi$. Strength curves were calculated using the two models based on the aforementioned parameters. Fig. 6 shows the calculation values (Zornberg and Michalowski models) and the test values at $D_r = 0.5$.

Figure 6 compared the S curves obtained using the two theoretical strength models and the measured values of S. It is demonstrated that the Zornberg model overestimated the S of the fibers, particularly at a relatively high ζ and long l_f. However, the values of S predicted by the Michalowski model were close to the measured values, which conform to results of Sadek *et al.* (2010). As shown in Eq. (11), φ_{eq} is directly proportional to the product of fiber content, length/diameter ratio and the coefficient of interaction between the fibers and sand and increases in proportion to the increase in ζ and η. At low ζ and η, the test value of S was slightly lower than that reflected by the theoretical S curve, and this difference increased in proportion to the increase in ζ and η. As demonstrated in Eq. (21), φ_{eq} is nonlinearly related to fiber content and length/diameter ratio. The two theoretical strength models are based on different assumptions. The equation for the S of FRS obtained based on the mode of failure of fibers assumed by each model contains only f but no c. Generally, sand has a low c, and its strength consists mainly of f. For the FRS, because of the interaction between the fibers and sand, the fibers generate a tensile force as a result of tensile deformation during the shear process, which is equivalent to the c between the sand particles. Because the fibers limit the dislocation and redistribution of the sand particles, the φ of the sand increases correspondingly. As demonstrated in Table 2, the FRS not only had a slightly high φ but also maintained a large c compared to the sand, demonstrating that the test results are in agreement with the analysis results. Therefore, the addition of fibers led to a significant change in the mechanical properties of the sand, which can be satisfactorily analyzed from a composite material perspective.

5. Conclusions

In this study, the mechanical properties of the FRS were thoroughly investigated through extensive triaxial consolidated drained tests. The focus was placed on the analysis of the effects of l_f, ζ, D_r and σ_3. Based on the triaxial test results, the Zornberg and Michalowski models were employed to predict the S of the FRS. The following conclusions were drawn from a comprehensive analysis of the test and model-calculated results:

1. The S of the FRS increased as l_f, ζ, σ_3 and D_r increased. The FRS displayed a hardening trend under the test loads and did not soften at a high strain level, which indicated that fibers reinforced the sand.
2. After adding fibers, the angle of internal friction φ increased slightly, and its c became high. At a fixed ζ, the c provided by long fibers was greater than that provided by short fibers, and long fibers also led to a significant increase in φ. Overall, the FRS possessed not only an f (its φ was slightly higher than that of the sand) but also a relatively high c.
3. The difference between the predicted results of Zornberg model and test results was significantly affected by the value of the parameter α. At a low ζ and a short l_f, the predicted values of Michalowski model were in good agreement with the measured values.

Acknowledgements

This study was supported by the Special Fund for Scientific Research by Xijing University (XJ18T01) and Special Fund for Scientific Research by Shaanxi Provincial Education Department (18JK1199).

ORCID

Gang Li https://orcid.org/0000-0003-0200-6097
Jinli Zhang https://orcid.org/0000-0002-6188-9750
Jia Liu https://orcid.org/0000-0002-2392-6629

References

Ahmad, F., Bateni, F., and Azmi, M. (2010). "Performance evaluation of silty sand reinforced with fibers." *Geotextiles and Geomembranes*, Vol. 28, No. 1, pp. 93-99, DOI: 10.1016/j.geotexmem.2009.09.017.

Claria, J. J. and Vettorelo, P. V. (2016). "Mechanical behavior of loose sand reinforced with synthetic fibers." *Soil Mechanics and Foundation Engineering*, Vol. 53, No. 1, pp. 12-18, DOI: 10.1007/s11204-016-9357-9.

Consoli, N. C., Casagrande, M. D. T., and Coop, M. R. (2005). "Effect of fiber reinforcement on the isotropic compression behavior of a sand." *Journal of Geotechnical and Geoenvironmental Engineering*, Vol. 131, No. 11, pp. 1434-1436, DOI: 10.1061/(ASCE)1090-0241(2005)131:11(1434).

Consoli, N. C., Casagrande, M. D. T., Prietto, P. D. M., and Thome, A. (2003). "Plate load test on fiber-reinforced soil." *Journal of Geotechnical and Geoenvironmental Engineering*, Vol. 129, No. 10, pp. 951-955, DOI: 10.1061/(ASCE)1090-0241(2003)129:10(951).

Consoli, N. C., Márcio, A. V., Fonini, A., and Rosa, F. D. (2009). "Fiber reinforcement effects on sand considering a wide cementation range." *Geotextiles and Geomembranes*, Vol. 27, No. 3, pp. 196-203, DOI: 10.1016/j.geotexmem.2008.11.005.

Diambra, A., Ibraim, E., Wood, D. M., and Russell, A. R. (2010). "Fiber reinforced sands: Experiments and modelling." *Geotextiles and Geomembranes*, Vol. 28, No. 3, pp. 238-250, DOI: 10.1016/j.geotexmem.2009.09.010.

Ding, J. H. and Bao, C. G. (1999). "Mechanical mechanism analysis of reinforced soil." *8th Conference on Soil Mechanics and Geotechnical Engineering*, Nanjing, China, pp. 441-444.

Gray, D. H. and Ohashi, H. (1983). "Mechanics of fiber reinforcement in sand." *Journal of Geotechnical Engineering*, Vol. 109, No. 3, pp. 335-353, DOI: 10.1061/(ASCE)0733-9410(1983)109:3(335).

Li, C. and Zornberg, J. G. (2013). "Mobilization of reinforcement forces in fiber-reinforced soil." *Journal of Geotechnical and Geoenvironmental Engineering*, Vol. 139, No. 1, pp. 107-115, DOI: 10.1061/(ASCE)

GT.1943-5606.0000745.

Maher, M. H. and Gary, D. H. (1990). "Static response of sands reinforced with randomly distributed fibers." *Journal of Geotechnical Engineering*, Vol. 116, No. 11, pp. 1661-1677, DOI: 10.1061/(ASCE)0733-9410(1990)116:11(1661).

Michalowski, R. L. and Cermak, J. (2003). "Triaxial compression of sand reinforced with fibers." *Journal of Geotechnical and Geoenvironmental Engineering*, Vol. 129, No. 2, pp. 125-136, DOI: 10.1061/(ASCE)1090-0241(2003)129:2(125).

Noorzad, R. and Amini, P. F. (2014). "Liquefaction resistance of babolsar sand reinforced with randomly distributed fibers under cyclic loading." *Soil Dynamics and Earthquake Engineering*, Vol. 66, pp. 281-292, DOI: 10.1016/j.soildyn.2014.07.011.

Ranjan, G., Vasan R. M., and Charan H. D. (1996). "Probabilistic analysis of randomly distributed fiber-reinforced soil." *Journal of Geotechnical Engineering*, Vol. 122, No. 6, pp. 419-426, DOI: 10.1061/(ASCE)0733-9410(1996)122:6(419).

Sadeghi, M. M. and Beigi, F. H. (2014). "Dynamic behavior of reinforced clayey sand under cyclic loading." *Geotextiles and Geomembranes*, Vol. 42, No. 5, pp. 564-572, DOI: 10.1016/j.geotexmem.2014.07.005.

Sadek, S., Najjar, S. S., and Freiha, F. (2010). "Shear strength of fiber-reinforced sands." *Journal of Geotechnical and Geoenvironmental Engineering*, Vol. 136, No. 3, pp. 490-499, DOI: 10.1061/(ASCE)GT.1943-5606.0000235.

Shewbridge, S. E. and Sitar, N. (1989). "Deformation characteristics of reinforced sand in direct shear." *Journal of Geotechnical Engineering*, Vol. 115, No. 8, pp. 1134-1147, DOI: 10.1061/(ASCE)0733-9410(1989)115:8(1134).

Shewbridge, S. E. and Sitar, N. (1990). "Deformation-based model for reinforced sand." *Journal of Geotechnical Engineering*, Vol. 116, No. 7, pp. 1153-1170, DOI: 10.1061/(ASCE)0733-9410(1990)116:7(1153).

Shewbridge, S. E. and Sitar, N. (1996). "Formation of shear zones in reinforced sand." *Journal of Geotechnical Engineering*, Vol. 122, No. 11, pp. 873-885, DOI: 10.1061/(ASCE)0733-9410(1996)122:11(873).

Shukla, S. K. (2017). *Fundamentals of fibre-reinforced soil engineering*, Springer Press, Berlin, Germany, DOI: 10.1007/978-981-10-3063-5.

Tang, C. S., Wang, D.Y., Cui, Y. J., Shi, B., and Li, J. (2016). "Tensile strength of fiber-reinforced soil." *Journal of Materials in Civil Engineering*, Vol. 28, No. 7, p. 04016031, DOI: 10.1061/(ASCE)MT.1943-5533.0001546.

Wang, Y. X., Guo, P. P., Dai, F., Li, X., Zhao, Y. L., and Liu, Y. (2018). "Behavior and modeling of fiber-reinforced clay under triaxial compression by combining the superposition method with the energy-based homogenization technique." *International Journal of Geomechanics*, Vol. 18, No. 12, p. 04018172, DOI: 10.1061/(ASCE)GM.1943-5622.0001313.

Wang, Y. X., Guo, P. P., Ren, W. X., Yuan, B. X., Yuan, H. P., Zhao, Y. L., Shan, S. B., and Cao, P. (2017). "Laboratory investigation on strength characteristics of expansive soil treated with jute fiber reinforcement." *International Journal of Geomechanics*, Vol. 17, No. 11, pp. 1-12, DOI: 10.1061/(ASCE)GM.1943-5622.0000998.

Yetimoglu, T. and Salbas, O. (2003). "A study on shear strength of sands reinforced with randomly distributed discrete fibers." *Geotextiles and Geomembranes*, Vol. 21, No. 2, pp. 103-110, DOI: 10.1016/S0266-1144(03)00003-7.

Zhang, Y. M., Zhang, X. D., and Zhang, H. R. (2005). "Test research of geotechnique textile soil reinforcement mechanism and engineering application." *Rock and Soil Mechanics*, Vol. 26, No. 8, pp. 1323-1326.

Zornberg, J. G. (2002). "Discrete framework for limit equilibrium analysis of fiber-reinforced soil." *Géotechnique*, Vol. 52, No. 8, pp. 593-604, DOI: 10.1680/geot.2002.52.8.593.